Spontaneous emission and absorption properties of a driven three-level system. II. The Λ and cascade models

A. S. Manka, H. M. Doss, L. M. Narducci,* and P. Ru†
Physics Department, Drexel University, Philadelphia, Pennsylvania 19104

G.-L. Oppo
Department of Physics and Applied Physics, University of Strathclyde, Glasgow G4 ONG, Scotland
(Received 21 September 1990)

This paper is concerned with the spectral profile of spontaneously emitted radiation from Λ and cascade models of driven three-level atoms, and with the absorption spectra of a weak probe. The atoms are excited by a pair of coherent external fields that are resonant or nearly resonant with the two dipole-allowed transitions of each of these two models. The main aim of this work is to extend earlier studies of the V-model configuration of three-level atoms and to present a comprehensive survey of the emission and absorption features of these systems. In addition to a derivation of exact formulas for the spectra and explicit analytic approximations in the high-intensity limit, we provide an explanation for the existence of simultaneous stationary population inversion between pairs of atomic levels and explore the effect of Doppler broadening on the absorption profile of the weak probe. In view of the latter analysis, in particular, we conclude that gain features persist even in the presence of inhomogeneous broadening. This suggests the possibility of experimental tests in a cell rather than an atomic-beam environment.

I. INTRODUCTION

The spontaneous emission from excited atoms, while a natural focus of early quantum mechanics, became an especially active area of research during the 1970s,[1–3] after the development of narrow-band tunable lasers. Today, it is again at the forefront of quantum optics research, following the recent advances in the construction of atomic traps[4] and the direct observation of emission and absorption of individual quanta from isolated atoms.[5] Thus, it is reasonable to expect that continued progress in experimental sophistication should provide even more refined measurements of resonance fluorescence than currently possible with atomic-beam technology, a prospect that adds impetus to our interest in finer theoretical details of the behavior of driven atoms.

In a recent paper[6] we proposed that the fluorescence spectrum of a driven pair of atomic levels can undergo significant changes when the lower state of the atomic transition is coupled to a third level by a second coherent field (the V model). The most significant modifications affect the total radiated intensity and the linewidths of its spectral components; the linewidths, in particular, become a mixture of the individual atomic-decay parameters with weight factors that depend on the strength of the applied fields. Thus, for example, under appropriate conditions the spontaneous-emission spectrum can become even narrower than expected on the basis of the ordinary Wigner-Weisskopf theory.[7] In fact, a recent experiment by Mossberg and collaborators[8] has provided a convincing verification of this prediction with a beam of Ba atoms driven by two narrow-band tunable dye lasers.

In addition to these features of the emission spectrum, our calculations have also shown interesting new facts concerning the absorption spectrum of a weak probe after it emerges from the interaction with a gas of driven atoms. It has been known for some time that a weak probe can be amplified as it propagates through a collection of driven two-level systems;[9] this gain manifests itself through the appearance of regions of negative absorption in the spectrum of the transmitted probe. The novelty of the predictions advanced in Ref. 6 is that the entire absorption profile can turn into a gain profile, a fact which is connected with the surprising appearance of steady-state population inversion between each of the two excited states of the V system and the ground level.

In the course of our study of the spectral properties of arbitrary three-level atoms we have discovered significant differences, and not just quantitative variations, between the behavior of V systems and the other two possible alternatives, the Λ (or inverted V) and the Ξ (or cascade) configurations (see Fig. 1). Because, experimentally, one structure may be more easily accessible than the others to the existing tunable sources of radiation, it may be useful to collect a brief survey of the behavior of the Λ and the Ξ models to complement the results presented in Ref. 6. The physical setting of interest is the same as that of Ref. 6, aside from the fact that different pairs of allowed transitions are coupled by the resonant driving fields. For this reason we limit our presentation to a sketch of the procedure and a description of the results, in the interest of providing a useful collection of theoretical guidelines for possible future experiments.

As in Ref. 6, here also we focus on the emission line shapes of the driven atoms and on the absorption spectrum of a weak probe using a standard master equation

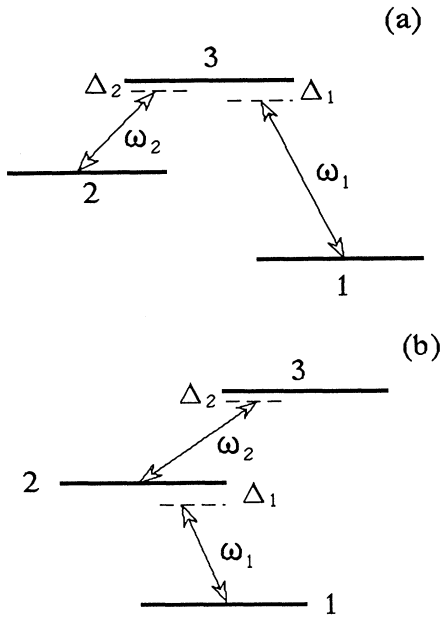

FIG. 1. Schematic representation of the (a) Λ model and (b) Ξ model; ω_1 and ω_2 are the carrier frequencies of the driving fields and Δ_1 and Δ_2 the respective detuning parameters.

approach and the regression theorem. In addition, we investigate some of the effects of inhomogenous broadening on the predicted line shapes, an aspect of the problem that we did not consider in our earlier work. As expected, the narrow features of the emission spectra are destroyed by inhomogeneous broadening, but some of the relevant absorption or gain features are preserved.

In Sec. II we describe the two models and derive their equations of motion. We analyze the emission and absorption spectra in Sec. III using a slightly different and somewhat more convenient procedure than adopted in Ref. 6. Section IV is devoted to a survey of the numerical results and to a comparison of the various predictions for the different atomic configurations. In this section we also discuss the effect of Doppler broadening on the absorption features of selected transitions. One of the unexpected conclusions of our calculations, as already mentioned, is the existence of a steady-state population inversion between each of the excited states and the lowest level; in Sec. V we develop a simple rate-equation argument to show that this phenomenon is related to competing Raman transitions in the three-level atoms. Considerable analytic progress can be made with the derivation of explicit spectral line shapes in a suitable high-intensity limit; in Sec. VI we show how this limit leads to the analytic derivation of simple formulas which we also list in detail for possible future reference. Section VII contains a summary of our results and some concluding comments.

II. DESCRIPTION OF THE MODEL AND EQUATIONS OF MOTION

We are interested in the evolution of two models of three-level atoms driven by coherent sources whose carrier frequencies are ω_1 and ω_2, as illustrated schematically in Figs. 1(a) and 1(b). The Λ model [Fig. 1(a)] is driven at the transition frequencies $1\rightarrow 3$ and $2\rightarrow 3$, while in the Ξ model levels $1\rightarrow 2$ and $2\rightarrow 3$ are coupled by the external fields [Fig. 1(b)]. A common feature of these systems, which makes them rather different from the V model, is that the field at frequency ω_2 has no effect on the atomic dynamics in the absence of the first, assuming of course that all the atoms are initially in their ground state and no other excitation mechanism in present.

In our description we adopt the semiclassical approximation in which the atomic degrees of freedom are described by appropriate fermion operators and the fields are c-number functions with Rabi frequencies g_1 and g_2. The levels that are coupled by the applied fields have dipole-allowed transitions so that, for reasons of parity, the $1\rightarrow 2$ transition of the Λ model and the $1\rightarrow 3$ transition of the Ξ model are forbidden. Decay rates W_{ij} $(i>j)$ characterize the spontaneous deexcitation of the higher levels, while upward rates $(i<j)$ are virtually zero because of the negligible thermal-excitation probability, as long as the energy spacing between levels is large, relative to kT.

The common unperturbed Hamiltonian of the Λ and Ξ models is

$$H_0=\sum_{i=1}^{3}\varepsilon_i a_i^\dagger a_i \ , \tag{2.1}$$

where ε_i $(i=1,2,3)$ are the energy eigenvalues of the isolated atoms and $a_i^\dagger$ and a_i are the fermion operators that describe the creation of an electron in level i or its removal. The two interaction Hamiltonians in the rotating-wave approximation are

$$H_1^\Lambda=\hbar g_1(e^{-\omega_1 t}a_3^\dagger a_1+e^{i\omega_1 t}a_1^\dagger a_3) +\hbar g_2(e^{-i\omega_2 t}a_3^\dagger a_2+e^{i\omega_2 t}a_2^\dagger a_3) \ , \tag{2.2a}$$

$$H_1^\Xi=\hbar g_1(e^{-i\omega_1 t}a_2^\dagger a_1+e^{i\omega_1 t}a_1^\dagger a_2) +\hbar g_2(e^{-i\omega_2 t}a_3^\dagger a_2+e^{i\omega_2 t}a_2^\dagger a_3) \ , \tag{2.2b}$$

where the Rabi frequencies g_1 and g_2 are real, for simplicity. The evolution of both systems in the interaction representation is governed by the master equation

$$\frac{\partial\rho'}{\partial t}=-\frac{i}{\hbar}[H_1',\rho']+\Lambda\rho' \ , \tag{2.3}$$

where H_1' denotes either $H_1^{\Lambda'}$ or $H_1^{\Xi'}$ in the interaction representation and $\Lambda\rho'$ is the irreversible part that describes the effects of spontaneous emission and, possibly, other collisional relaxation processes. The specific form of the irreversible term for an arbitrary multilevel system[10] is

$$\Lambda\rho'=\sum_{i,j}[a_i^\dagger a_j\rho' a_j^\dagger a_i(A_{jiij}+A_{jiij}^*) -a_j^\dagger a_j\rho' A_{jiij}-\rho' a_j^\dagger a_j A_{jiij}^*] \ , \tag{2.4}$$

where A_{jiij} are complex rate constants related to the population transition rates W_{ij}, the polarization decay rates γ_{ij}, and the frequency shifts $\Delta\Omega_{ij}$ by the equations

$$W_{ij}=A_{jiij}+A^{*}_{jiij}\ , \tag{2.5a}$$

$$\gamma_{ij}=\sum_k \mathrm{Re}(A_{ikki}+A^{*}_{jkkj})$$

$$=\tfrac{1}{2}\sum_k (W_{ik}+W_{jk})\ , \tag{2.5b}$$

$$\Delta\Omega_{ij}=-\sum_k \mathrm{Im}(A_{jkkj}+A^{*}_{ikki})\ . \tag{2.5c}$$

In the following we shall ignore both level shifts and pure phase-relaxation effects due to elastic collisions, i.e., we assume $\Delta\Omega_{ij}=0$ and $A_{iiii}=0$.

The master equation (2.3), when written in terms of the matrix elements ρ'_{ij}, yields nine coupled linear equations of which only eight are linearly independent by virtue of the trace condition, $\mathrm{Tr}\rho'=1$. These equations contain time-dependent oscillating factors that we must eliminate in order to apply the regression theorem in the convenient form described below. This step can be accomplished by a suitable redefinition of the relevant variables, as summarized in the Appendix, and the final result can be cast in the form of the compact vector equation

$$\frac{d}{d\tau}\boldsymbol{\psi}(\tau)=L\boldsymbol{\psi}(\tau)+\mathbf{I}\ , \tag{2.6}$$

where $\tau=W_{31}t$ for the Λ model and $\tau=W_{21}t$ for the Ξ model. The two Rabi frequencies are also scaled into dimensionless form by using W_{31} or W_{21}, respectively, as the unit rates. The same is done with the remaining rate constants of the problem whose scaled versions will be labeled with a "tilde" in the following discussion. The relation between the eight components ψ_i of the column vector $\boldsymbol{\psi}$ and the original matrix elements ρ'_{ij} is listed in the Appendix. The inhomogeneous vector $\mathbf{I}$ that appears in Eq. (2.6) originates from the elimination of ρ'_{11} from Eq. (2.3) and its replacement with $1-\rho'_{22}-\rho'_{33}$, according to the trace condition. Its explicit form is also listed in the Appendix.

We do not need to worry about the explicit time-dependent solution of Eq. (2.6) (except formally in our implementation of the regression theorem), but we do need the steady-state solution. This is given by

$$\boldsymbol{\psi}(\infty)=-L^{-1}\mathbf{I}\ , \tag{2.7a}$$

or, in component form, by

$$\psi_i(\infty)=-\sum_j (L^{-1})_{ij}I_j\ . \tag{2.7b}$$

III. THE CALCULATION OF THE SPECTRA

We begin with the construction of the spectrum of the spontaneously emitted radiation. This is given by the Fourier transform of the field-correlation function

$$\gamma(\tau_1,\tau_0)=\langle \mathbf{E}^{(-)}(\mathbf{r},\tau_1)\cdot\mathbf{E}^{(+)}(\mathbf{r},\tau_2)\rangle\ , \tag{3.1}$$

where $\mathbf{E}^{(\pm)}$ denotes, respectively, the positive and negative parts of the total-field operator at the observation point $\mathbf{r}$, measured from the position of the scattering center. Because the master equation (2.3) involves only atomic operator degrees of freedom, we need a relation between these and the scattered quantum field; in the far zone, this is provided by the well-known formula

$$\mathbf{E}^{(+)}(\mathbf{r},t)=\mathbf{E}_0^{(+)}(\mathbf{r},t)-\frac{\omega_0^2}{c^2 r}\hat{\mathbf{n}}\times(\hat{\mathbf{n}}\times\hat{\mathbf{d}})P^{(+)}\left[t-\frac{r}{c}\right]\ , \tag{3.2}$$

together with its Hermitian adjoint, where $\mathbf{E}_0^{(+)}$ is the positive-frequency part of the solution of the homogeneous wave equation, ω_0 is the frequency of the incident field, $\hat{\mathbf{n}}$ is the unit vector in the direction of observation, and $\hat{\mathbf{d}}$ is the unit vector along the atomic dipole moment.

Because our setting involves simultaneously two different fields, usually with very different carrier frequencies, each field generates a scattered contribution of the type (3.2), after inducing an appropriate atomic polarization. The positive-frequency parts of the polarization operators for the Λ model are

$$P_{\Lambda 1}^{(+)}=\mu_{13}a_1^{\dagger}a_3,\quad P_{\Lambda 2}^{(+)}=\mu_{23}a_2^{\dagger}a_3\ , \tag{3.3a}$$

where the indices 1 and 2 in $P_{\Lambda}^{(+)}$ refer to the two driving fields [see Fig. 1(a)]; for the Ξ model they are

$$P_{\Xi 1}^{(+)}=\mu_{12}a_1^{\dagger}a_2,\quad P_{\Xi 2}^{(+)}=\mu_{23}a_2^{\dagger}a_3\ . \tag{3.3b}$$

The symbols μ_{ij} denote the magnitudes of the transition dipole moments between levels i and j.

In view of Eq. (3.2), and apart from numerical factors that we need not specify for our purposes, the required correlation functions have the general form

$$\Gamma(\tau_1,\tau_0)=\langle P^{(-)}(\tau_1)P^{(+)}(\tau_0)\rangle\ . \tag{3.4}$$

As already shown in Ref. 6, a convenient way to handle the two-time expectation value (3.4) is by way of the regression theorem.[11] We outline the procedure adopted in this calculation for one specific case [one of the four listed in Eqs. (3.3)] following a slightly different and perhaps more transparent procedure than in Ref. 6. Thus for the purpose of illustration, consider the correlation function

$$\Gamma_{\Lambda 1}(\tau_1,\tau_0)=\mu_{13}^2\langle P_{\Lambda 1}^{(-)}(\tau_1)P_{\Lambda 1}^{(+)}(\tau_0)\rangle\ . \tag{3.5}$$

The starting point is the evaluation of the single-time average $\langle P_{\Lambda 1}^{(-)}(\tau_1)\rangle$ whose explicit form is

$$\langle P_{\Lambda 1}^{(-)}(\tau_1)\rangle=\mathrm{Tr}[\rho(\tau_1)P_{\Lambda 1}^{(-)}]=\mu_{13}\exp(+\tilde{\omega}_1\tau_1)\psi_2(\tau_1)\ , \tag{3.6}$$

where $\tilde{\omega}_1$ denotes ω_1/W_{31}. The formal solution of eq. (2.6) is

$$\boldsymbol{\psi}(\tau_1)=\exp[L(\tau_1-\tau_0)]\boldsymbol{\psi}(\tau_0)+\int_{\tau_0}^{\tau_1}d\tau'\exp[L(\tau_1-\tau')]\mathbf{I}\ , \tag{3.7}$$

and the polarization expectation value (3.6) can be written explicitly in terms of the "initial conditions" $\psi_j(\tau_0)$ $(j=1,\ldots,8)$ as follows:

$$\langle P_{\Lambda 1}^{(-)}(\tau_1)\rangle=\mu_{13}\exp(i\tilde{\omega}_1\tau_1)\sum_j\left[\{\exp[L(\tau_1-\tau_0)]\}_{2j}\psi_j(\tau_0)+\int_{\tau_0}^{\tau_1}d\tau'\{\exp[L(\tau_1-\tau')]\}_{2j}I_j\right] . \tag{3.8}$$

The next step in the application of the regression theorem is to cast the initial values $\psi_j(\tau_0)$ in the form of expectation values of suitable system operators. Thus, for example, with the help of Eqs. (A3), we have

$$\psi_1(\tau_0)=\exp[-i(\tilde{\omega}_1-\tilde{\omega}_2)\tau_0]\rho_{12}(\tau_0)$$
$$=\exp[-i(\tilde{\omega}_1-\tilde{\omega}_2)\tau_0]\langle|2\rangle\langle 1|\rangle_{\tau_0} . \tag{3.9}$$

Now we carry out the replacement

$$\langle|2\rangle\langle 1|\rangle_{\tau_0}\rightarrow\langle|2\rangle\langle 1|P_{\Lambda 1}^{(+)}(\tau_0)\rangle , \tag{3.10a}$$

leading to

$$\langle|2\rangle\langle 1|P_{\Lambda 1}^{(+)}(\tau_0)\rangle=\mu_{13}\exp[-i(\tilde{\omega}_1-\tilde{\omega}_2)\tau_0]\rho_{32}(\tau_0)$$
$$=\mu_{13}\exp(-i\tilde{\omega}_2\tau_0)\psi_7(\tau_0) . \tag{3.10b}$$

Similar calculations must be performed for the remaining elements of $\boldsymbol{\psi}(\tau_0)$. With respect to the inhomogeneous term, which contains no dependence on $\boldsymbol{\psi}(\tau_0)$, the appropriate replacement analogous to (3.10a) is

$$1\equiv\langle 1\rangle_{\tau_0}\rightarrow\langle P_{\Lambda 1}^{(+)}(\tau_0)\rangle=\mu_{13}\exp(-i\tilde{\omega}_1\tau_0)\psi_6(\tau_0) . \tag{3.11}$$

Finally the required correlation function takes the form

$$\Gamma_{\Lambda 1}(\tau_1,\tau_0)=\mu_{13}^2\exp(i\tilde{\omega}_1\tau)\left[M_{21}(\tau)\psi_7(\tau_0)+M_{22}(\tau)\psi_8(\tau_0)+\sum_{j=1}^{8}\int_{\tau_0}^{\tau_1}d\tau' M_{2j}(\tau_1-\tau')I_j\psi_6(\tau_0)\right] , \tag{3.12}$$

where

$$\tau=\tau_1-\tau_0,\quad M_{ij}(\tau)=(e^{L\tau})_{ij} . \tag{3.13}$$

We note that $\Gamma_{\Lambda 1}$ in Eq. (3.12) depends upon τ_1 and τ_0 only through their difference τ. At this point we take the limit $\tau_1,\tau_0\rightarrow\infty$ with τ arbitrary, and obtain the required asymptotic form.

For the purpose of a numerical calculation of the Fourier transform of Eq. (3.12) the best procedure is to take, first, the Laplace transform of the correlation function. This has a general structure of the form

$$\hat{\Gamma}_{\Lambda 1}(z)=A(z-i\tilde{\omega}_1)+\frac{1}{z-i\tilde{\omega}_1}B(z-i\tilde{\omega}_1) , \tag{3.14}$$

where A and B are analytic functions of z for $\mathrm{Re}z\geq 0$. The singularity at $z=0$ is the symptom of a coherent contribution to the spectrum, centered at ω_1, whose origin can be traced to the elastic scattering of the driving field (Rayleigh peak). The incoherent part of the spectrum, which is the dynamically relevant contribution, can be calculated by subtraction of the coherent peak through the algorithm

$$\hat{\Gamma}_{\Lambda 1}^{\mathrm{incoh}}(z)=\hat{\Gamma}_{\Lambda 1}(z)-\frac{1}{z-i\tilde{\omega}_1}\lim_{z\rightarrow i\tilde{\omega}_1}(z-i\tilde{\omega}_1)\hat{\Gamma}_{\Lambda 1}(z) . \tag{3.15}$$

The result of this simple calculation is (for $3\rightarrow 1$ emission)

$$\hat{\Gamma}_{\Lambda 1}^{\mathrm{incoh}}(z)=\mu_{13}^2\left[\hat{M}_{21}(z_1)\psi_7(\infty)+\hat{M}_{22}(z_1)\psi_8(\infty)+\sum_{j=1}^{8}\hat{N}_{2j}(z_1)I_j\psi_6(\infty)\right] , \tag{3.16}$$

where

$$z_1=z-i\tilde{\omega}_1 ,$$
$$\hat{M}_{ij}(z)=(z-L)_{ij}^{-1} ,$$
$$\hat{N}_{ij}(z)=[L^{-1}(z-L)^{-1}]_{ij} .$$

Finally, the spectrum of the fluorescent light is given by

$$S(\omega)=\mathrm{Re}\hat{\Gamma}_{\Lambda 1}^{\mathrm{incoh}}(z)|_{z=i\tilde{\omega}} . \tag{3.17}$$

The same procedure can be applied to the three remaining polarization operators, with the results (for $3\rightarrow 2$ emission)

$$\hat{\Gamma}_{\Lambda 2}^{\mathrm{incoh}}(z)=\mu_{23}^2\left[\hat{M}_{53}(z_2)\psi_6(\infty)+\hat{M}_{54}(z_2)\psi_7(\infty)+\hat{M}_{55}(z_2)\psi_8(\infty)+\sum_{j=1}^{8}\hat{N}_{5j}(z_2)I_j\psi_7(\infty)\right] , \tag{3.18}$$

where

$$z_2=z-i\tilde{\omega}_2$$

(for $2\rightarrow 1$ emission)

$$\hat{\Gamma}_{\Xi 1}^{\mathrm{incoh}}(z)=\mu_{12}^2\left[\hat{M}_{11}(z_1)\psi_4(\infty)+\hat{M}_{12}(z_1)\psi_5(\infty)+\sum_{j=1}^{8}\hat{N}_{1j}(z_1)I_j\psi_3(\infty)\right] , \tag{3.19}$$

and (for $3\rightarrow 2$ emission)

$$\hat{\Gamma}_{\Xi 2}^{\mathrm{incoh}}(z)=\mu_{23}^2\left[\hat{M}_{53}(z_2)\psi_6(\infty)+\hat{M}_{54}(z_2)\psi_7(\infty)+\hat{M}_{55}(z_2)\psi_8(\infty)+\sum_{j=1}^{8}\hat{N}_{5j}(z_2)I_j\psi_7(\infty)\right] . \tag{3.20}$$

Aside from the superficial similarity in the structure of the four emission spectra, which extends also to the case of the V model (Ref. 6), it is not possible to draw much useful information by simple inspection of these results. However, these equations are well suited for numerical calculations which only require standard matrix manipulation techniques. In Sec. IV we discuss characteristic samples of the exact emission spectra and compare these results with those derived in Ref. 6. In the limit of strong driving fields, it is possible to extract approximate analytic line shapes, as we discuss in Sec. VI.

Now we turn our attention to the calculation of the absorption spectra. The physical setting is the same as in the previous calculation, with the addition of a tunable weak probe passing through the driven atoms. The transmitted intensity of the probe is related to the incident intensity by the usual Beer law

$$I_{\rm out}=I_{\rm in}e^{A(\omega)L}\ , \tag{3.21}$$

where L is the length of the sample and $A(\omega)$ is the attenuation coefficient at the frequency ω of the probe. Usually $A(\omega)$ is negative and, of course, frequency dependent. If $A(\omega)>0$, the probe is amplified. According to linear-response theory,[9] $A(\omega)$ is connected to the atomic polarization operators according to the relation

$$A(\omega)=\text{const}\times\mathcal{F}\{\langle[P^{(-)}(\tau_1),P^{(+)}(\tau_0)]\rangle\}\ , \tag{3.22}$$

where $\mathcal{F}$ denotes the Fourier-transform operator, and the square brackets indicate the unequal time commutator. The expectation value must be computed under steady-state conditions, as in the case of the emission spectra.

Of the two contributions originating from the commutator, the first was already calculated in the first part of this section. The second can be handled in a similar way with the help of the regression theorem. Once again, depending upon the selected range of the tunable frequency ω, one or the other of the polarization operators listed in (3.3a) and (3.3b) come into play for each of the two models.

The required results, in Laplace transform space, are (for $1\rightarrow3$ absorption)

$$\begin{aligned}\hat{A}_{\Lambda1}(z)=\mu_{13}^2\{&\hat{M}_{21}(z_1)\psi_7(\infty)\\&+\hat{M}_{22}(z_1)[2\psi_8(\infty)+\psi_4(\infty)-1]\\&-\hat{M}_{25}(z_1)\psi_3(\infty)-\hat{M}_{28}(z_1)\psi_6(\infty)\}\ ,\end{aligned} \tag{3.23}$$

(for $2\rightarrow3$ absorption)

$$\begin{aligned}\hat{A}_{\Lambda2}(z)=\mu_{23}^2\{&\hat{M}_{53}(z_2)\psi_6(\infty)-\hat{M}_{52}(z_2)\psi_1(\infty)\\&+\hat{M}_{55}(z_2)[\psi_8(\infty)-\psi_4(\infty)]\\&+[\hat{M}_{54}(z_2)-\hat{M}_{58}(z_2)]\psi_7(\infty)\}\ ,\end{aligned} \tag{3.24}$$

(for $1\rightarrow2$ absorption)

$$\begin{aligned}\hat{A}_{\Xi1}(z)=\mu_{12}^2\{&\hat{M}_{11}(z_1)[2\psi_4(\infty)+\psi_8(\infty)-1]\\&+\hat{M}_{12}(z_1)\psi_5(\infty)-\hat{M}_{14}(z_1)\psi_3(\infty)\\&-\hat{M}_{17}(z_1)\psi_6(\infty)\}\ ,\end{aligned} \tag{3.25}$$

and (for $2\rightarrow3$ absorption)

$$\begin{aligned}\hat{A}_{\Xi2}(z)=\mu_{23}^2\{&\hat{M}_{53}(z_2)\psi_6(\infty)-\hat{M}_{52}(z_2)\psi_1(\infty)\\&+[\hat{M}_{54}(z_2)-\hat{M}_{58}(z_2)]\psi_7(\infty)\\&+\hat{M}_{55}(z_2)[\psi_8(\infty)-\psi_4(\infty)]\}\ .\end{aligned} \tag{3.26}$$

The actual absorption spectrum is related to $\hat{A}(z)$ by

$$A(\omega)=\text{Re}\,\hat{A}(z)|_{z=i\tilde{\omega}}\ . \tag{3.27}$$

We present selected results of the numerical evaluation of the absorption spectra in the next section.

IV. A SURVEY OF THE NUMERICAL RESULTS

This section contains a collection of selected numerical evaluations of the emission and absorption spectra derived in Sec. III and, when appropriate, a comparison with the results of our earlier studies of the V model (Ref. 6). Because, in the calculations listed in Sec. III, the time variable is scaled according to $\tau=Wt$, with $W=W_{31}$ for the Λ model, and $W=W_{21}$ for the Ξ model, the irreversible decay rates and frequencies are all given in units of W as well. Thus the Rabi frequencies are $\beta_i=g_i/W$ with $i=1,2$ and in particular, the frequency that appears along the horizontal axis of the figures is defined by

$$\tilde{\omega}=\begin{cases}\omega/W_{31} & \text{for the } \Lambda \text{ model}\\ \omega/W_{21} & \text{for the } \Xi \text{ model}\ .\end{cases}$$

For simplicity we have carried out the following calculations under resonant conditions, i.e., for example with $\omega_1=\omega_{31}$ and $\omega_2=\omega_{32}$ for the Λ model. Out of resonance, the spectra lose their symmetry and acquire additional peaks.

We begin with a typical emission spectrum for the $3\rightarrow1$ transition of the Λ model and a comparison with the spectrum that would result in the presence of only one driving field. In the latter case, of course, the spectral profile is not exactly the same as with an ideal two-level atom because of the extra decay pathway from the excited state of our system, but the differences are mainly quantitative in character. Thus, in Fig. 2(a) we show the spectrum of the driven three-level system with $\beta_1=4$ and $\beta_2=1$; this is to be compared with Fig. 2(b), a situation where $\beta_2=0$. The only obvious difference between these two curves is the appearance of an extra pair of sidebands in the first case, but we see no significant change in the linewidths. This is very different from the case of the V model (see, for example, Fig. 3 of Ref. 6) where the central peak of the three-level spectrum can be much narrower than that of the corresponding two-level system.

In Fig. 2(c) we reverse the relative strengths of the driving field and enhance the inner pair of sidebands, which now become the dominant features. The spacing of the sidebands from the central peak is related to the Rabi frequencies of the driving fields. As shown analytically in Sec. VI under high field conditions, the inner sidebands are removed from the center of the line by amounts

$$\Delta\tilde{\omega}=\pm(\beta_1^2+\beta_2^2)^{1/2} \tag{4.1}$$

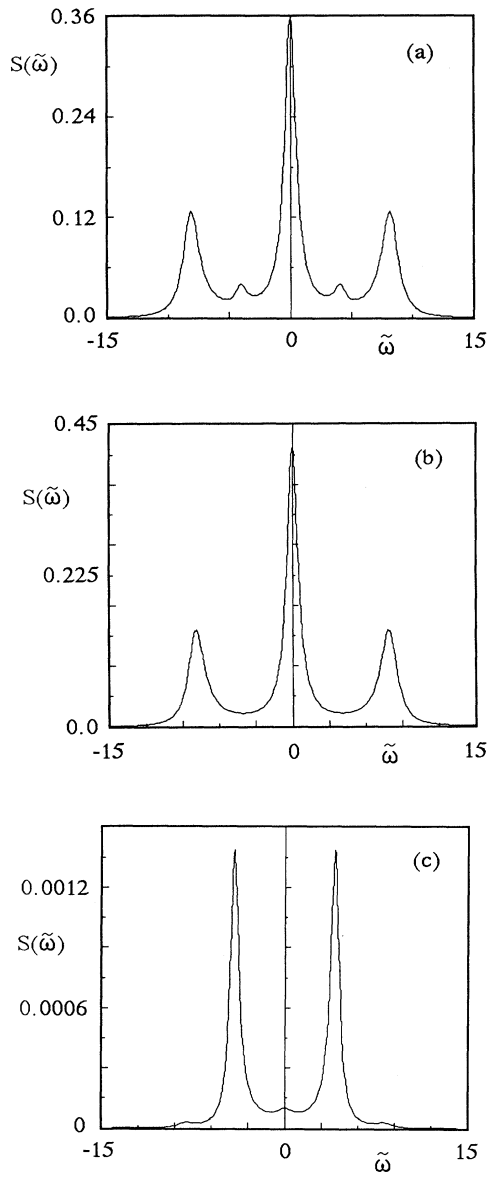

FIG. 2. The spontaneous-emission spectrum of the $3\rightarrow 1$ transition of the Λ model for $\bar{W}_{21}=0.5$, $\bar{W}_{32}=0.1$, and for (a) $\beta_1=4$, $\beta_2=1$; (b) $\beta_1=4$, $\beta_2=0$; and (c) $\beta_1=1$, $\beta_2=4$.

while the outer sidebands are twice as far away. The asymptotic result (4.1), which is accurate only under high field conditions, remains acceptable even for smaller values of the Rabi frequencies.

Thus, line narrowing effects do not emerge prominently in the Λ model (although line-broadening effects can occur, as described analytically in Sec. VI). With this atomic configuration, however, as $W_{21}\rightarrow 0$, the total fluorescence intensity is not only reduced but actually completely suppressed as a result of population trapping. This is not a desirable feature for the purpose of observation, but is unavoidable as shown experimentally under resonance conditions by several authors and by Gray, Whitley, and Stroud[12] in particular.

The emission spectra from the driven Ξ system show qualitatively similar features. In Figs. 3(a) and 3(b) we show the spectral profiles of the $2\rightarrow 1$, and $3\rightarrow 2$ spontaneous decays, respectively. Both, as in the case of the Λ model, have five components, and the latter [Fig. 3(b)] displays strongly enhanced inner sidebands. The outer sidebands are the three-level analogue of the sidebands of a driven two-level system, in the sense that they persist as the strength of one field approaches zero; thus, the inner spectral components are a characteristic signature of the multilevel nature of the driven atom. Unlike the Λ system, however, the Ξ model displays some limited amount of central-peak narrowing for the $3\rightarrow 2$ decay, as we can best see by inspection of Fig. 11(b) (see Sec. VI).

We now turn our attention to the absorption spectra of a tunable weak probe. These, of course, involve two different structures centered at the two resonant absorption frequencies $1\rightarrow 3$ and $2\rightarrow 3$ for the Λ model and $1\rightarrow 2$ and $2\rightarrow 3$ for the Ξ model. Just as in the case of the V model, the Λ system yields mixed absorption and gain features for appropriate choices of the driving field amplitudes with generally similar features, and it also displays the surprising appearance of a complete gain profile under high-field conditions. One example of this situation is shown in Fig. 4 for the $2\rightarrow 3$ transition. The $1\rightarrow 3$ spectrum also shows gain for every frequency of the tunable probe, although, in this case the maximum gain coefficient is smaller than the one shown in Fig. 4. The explanation for this result can be traced to the existence

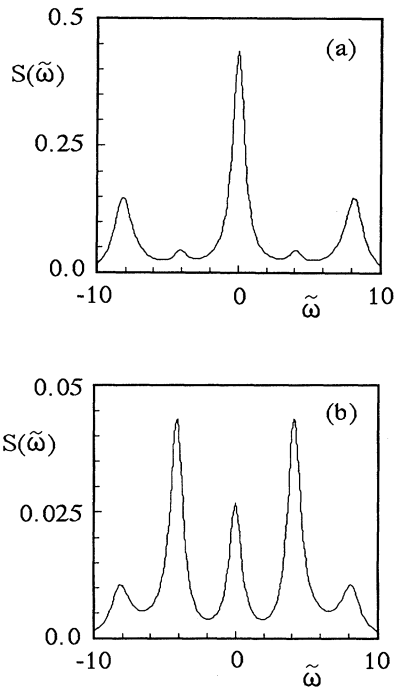

FIG. 3. The spontaneous-emission spectrum of the (a) $2\rightarrow 1$ transition and (b) $3\rightarrow 2$ transition of the Ξ model for $\bar{W}_{32}=0.5$, $\bar{W}_{31}=0.1$ and field strengths $\beta_1=4$ and $\beta_2=1$.

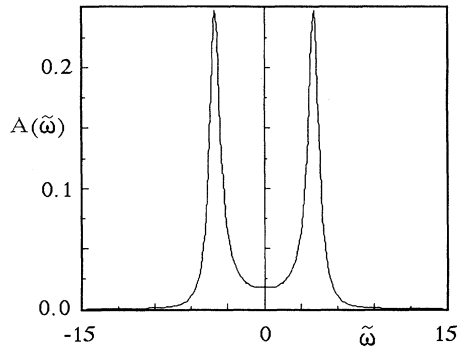

FIG. 4. The gain profile of the absorption spectrum for the $2\rightarrow 3$ transition of the Λ model with $\tilde{W}_{21}=0.5$, $\tilde{W}_{32}=0.1$ and $\beta_1=4$, $\beta_2=1$.

of steady-state conditions in which both the $3\rightarrow 1$ and $3\rightarrow 2$ transitions have population inversion (the $3\rightarrow 1$ population difference is much smaller than the one for the $3\rightarrow 2$ pair of levels). In Sec. V we review the origin of this effect which is absent in a driven two-level system.

The absorption spectrum of the Ξ model offers a surprise because simultaneous inversion of both allowed transitions is not possible. Thus, Figs. 5(a) and 5(b) show a gain profile for the $2\rightarrow 3$ weak-probe spectrum and the absorption profile for the companion $1\rightarrow 2$ transition, respectively. Again, in Sec. V we explain the origin of this phenomenon and the reasons for the differences between the behavior of the V and Λ models relative to that of the Ξ system.

So far our calculations have focused on a case in which the atoms can be simulated as homogeneously broadened radiators; this is typical of situations where well-collimated atomic beams are driven by equally well-collimated laser beams, directed orthogonally to the velocity vector of the atoms, and the direction of observation is also perpendicular to both atoms and fields. In the presence of misalignments from the ideal geometry, or in a cell environment, Doppler broadening becomes a dominant spectral feature for gaseous systems. It is not surprising that the presence of Doppler broadening erases all the interesting structures from the emission spectrum; it is rather surprising, instead, that significant aspects of the absorption (or gain) features are preserved. For this reason we close this section with a brief survey of the effect of Doppler broadening on the absorption spectra of a weak probe.

In this calculation we consider a collection of independent homogeneous systems and simulate their motion with appropriate detunings from line center; because each atom undergoes two different absorption or emission processes, we select the ratio of the two detuning coefficients to match the chosen ratio of the transition frequencies (in line with the first-order Doppler formula). Each homogeneous "packet" yields a different spectral profile which we weigh with the Maxwell-Boltzmann factor to amount for the velocity distribution. The required total spectrum is the incoherent superposition of all the individual line shapes.

For definiteness, we also assume that the driving fields are exactly resonant with the atoms that are stationary (or that move exactly perpendicular) with respect to the driving fields. We take a Doppler velocity distribution with ten homogeneous packets for each standard deviation, and extend the distribution of the velocities to three standard deviations on each side of the maximum. Thus, the spectral averaging process includes 61 different packets of homogeneously broadened atoms.

In Fig. 6 we show a typical absorption spectrum of the $2\rightarrow 3$ transition of the Λ model with and without

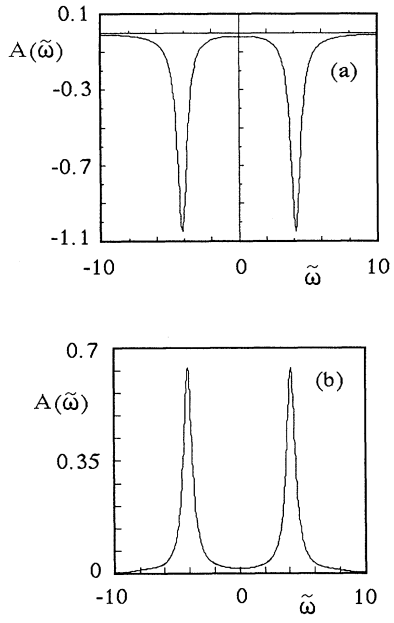

FIG. 5. The absorption spectrum of the (a) $1\rightarrow 2$ transition of the Ξ model, showing absorption at all probe frequencies, and (b) $2\rightarrow 3$ transition displaying gain. The parameters are $\tilde{W}_{31}=0.1$, $\tilde{W}_{32}=0.5$, zero detunings, $\beta_1=1$, and $\beta_2=4$.

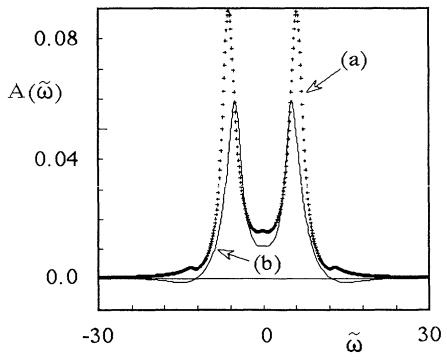

FIG. 6. The Doppler effect on the $2\rightarrow 3$ transition of the Λ model for $\tilde{W}_{21}=2.0$ $\tilde{W}_{32}=0.5$, $\beta_1=6$, and $\beta_2=2$. Curve (a) represents the spectrum without Doppler broadening and curve (b) with the Doppler effect.

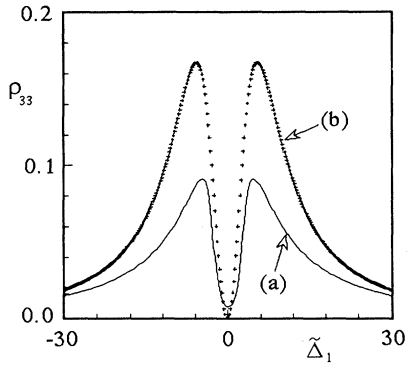

FIG. 7. Population trapping in level 3 of the Λ model as a function of the scaled frequency detuning between the driving field 1 and the atomic transition frequency ($\tilde{W}_{21}=0$, $\tilde{W}_{32}=1.0$, $\beta_1=3$, $\beta_2=1$, and zero detunings) with (a) and without (b) Doppler broadening. The trapping is almost complete with the Doppler effect, but the excited population is significantly lower.

Doppler-broadening effects. Clearly the main feature of the ideal homogeneous case (i.e., the presence of a completely positive absorption line) is preserved fairly accurately and gain should be observable even in a cell environment. The same is not true for the $1\rightarrow 3$ transition, perhaps because of the much smaller population inversion between these levels under high-field conditions. We have also verified that the population-trapping effect is preserved, although it is reduced somewhat in the presence of inhomogeneous broadening (Fig. 7).

V. STATIONARY POPULATION DISTRIBUTIONS OF THE DRIVEN ATOMS

It is well known that two-level atoms cannot be driven in a state of inversion under stationary conditions, regardless of the strength of the driving field. A transient inversion can be produced with a resonant π pulse if its duration is sufficiently shorter than the atomic relaxation times of the polarization and population. Of course the notion of stationary population inversion in a multilevel atom is as old as the laser, but apparently not until recently have we begun to appreciate that both allowed transitions of a three-level system can be driven into a state of inversion. The origin of the fully positive gain profiles for both $1\rightarrow 2$ and $1\rightarrow 3$ transitions of the V model and the $2\rightarrow 3$ and $1\rightarrow 3$ transitions of the Λ model is rooted in this effect. This phenomenon is rather counterintuitive if one tries to understand it only on the basis of standard arguments based upon Einstein transition rates and competition with the spontaneous-decay processes. Evidence of its nontrivial character is offered, for example, by the fact that the V and Λ models share the common ability to support pairs of inverted levels, but not the Ξ model.

Actually, the origin of this effect can be understood using the standard density-matrix equations listed in the Appendix, although the most direct way to demonstrate it is with the help of the dressed atomic states (see Sec. VI). Here we offer a concise survey of the lengthy but elementary calculations for the cases of the Λ and Ξ systems. For simplicity, we restrict our attention to resonant interaction between the fields and the atoms.

With reference to the density-matrix equations for the Λ model [Eq. (A1)] listed in the Appendix, we consider the stationary solutions of the polarization equations for the variables ρ'_{12}, ρ'_{13} and ρ'_{23}: they have the form

$$\rho'_{12}=\frac{1}{D}\left[\frac{g_1g_2}{\gamma_{23}}D_{32}+\frac{g_1g_2}{\gamma_{13}}D_{31}\right], \tag{5.1a}$$

$$\rho'_{13}=-i\frac{g_1}{\gamma_{13}}D_{31}\left[1-\frac{g_2^2}{\gamma_{13}D}\right]+i\frac{g_1g_2^2}{\gamma_{13}\gamma_{23}D}D_{32}, \tag{5.1b}$$

$$\rho'_{32}=i\frac{g_2}{\gamma_{23}}D_{32}\left[1-\frac{g_1^2}{\gamma_{23}D}\right]-i\frac{g_1^2g_2}{\gamma_{13}\gamma_{23}D}D_{31}, \tag{5.1c}$$

where $D_{ij}=\rho'_{ii}-\rho'_{jj}$, and

$$D=\gamma_{12}+\frac{g_1^2}{\gamma_{23}}+\frac{g_2^2}{\gamma_{13}}. \tag{5.2}$$

Next, we substitute Eqs. (5.1) into the population equations for ρ'_{11} and ρ'_{22} (there is no need to consider ρ'_{33} because of the trace condition $\rho'_{11}+\rho'_{22}+\rho'_{33}=1$) and obtain

$$\frac{d\rho'_{11}}{dt}=B_{13}D_{31}-\mathcal{R}D_{32}+W_{21}\rho'_{22}+W_{31}\rho'_{33}, \tag{5.3a}$$

$$\frac{d\rho'_{22}}{dt}=B_{23}D_{32}-\mathcal{R}D_{31}+W_{32}\rho'_{33}-W_{21}\rho'_{22}, \tag{5.3b}$$

where

$$B_{13}=\frac{2g_1^2}{\gamma_{13}D}\left[\gamma_{12}+\frac{g_1^2}{\gamma_{23}}\right], \tag{5.4a}$$

$$B_{23}=\frac{2g_2^2}{\gamma_{23}D}\left[\gamma_{12}+\frac{g_2^2}{\gamma_{13}}\right], \tag{5.4b}$$

$$\mathcal{R}=\frac{2g_1^2g_2^2}{\gamma_{13}\gamma_{23}D}. \tag{5.4c}$$

At this point it is easy to see [Eq. (5.3)] that the population dynamics is controlled by absorption and stimulated emission coefficients, B_{13} and B_{23}, for the two driving fields, by the spontaneous-decay rates, and by terms that depend on the product of the two field intensities [Eq. (5.4c)]. These terms play the role of Raman transition rates and reflect the coupling induced between levels 1 and 2 by their common coherent interaction with level 3.

Now we express the population variables ρ'_{ii} in Eqs. (5.3) in terms of the population differences D_{31} and D_{32} and solve in steady state after making the simplifying assumption that the Rabi frequencies of the fields are much larger than the decay rates (this is also the condition of greatest interest where our numerical solutions of the absorption spectra exhibit gain for all frequencies). The result is

$$D_{31}=\frac{1}{3}\frac{\mathcal{R}(W_{21}-W_{32})-B_{23}(W_{31}+W_{21})}{2\mathcal{R}\gamma_{12}}, \tag{5.5a}$$

$$D_{32}=\frac{1}{3}\frac{B_{13}(W_{21}-W_{32})-\mathcal{R}(W_{31}+W_{21})}{2\mathcal{R}\gamma_{12}} . \quad (5.5b)$$

Simultaneous inversion can be obtained if the following inequalities are satisfied:

$$\frac{W_{21}-W_{32}}{W_{31}+W_{21}}>\frac{B_{23}}{\mathcal{R}} \quad (D_{31}>0) \quad (5.6a)$$

$$\frac{W_{21}-W_{32}}{W_{31}+W_{21}}>\frac{\mathcal{R}}{B_{13}} \quad (D_{32}>0) \quad (5.6b)$$

and because $B_{23}B_{13}>\mathcal{R}^2$ [as we can easily verify from Eqs. (5.4)], it follows that

$$\frac{B_{23}}{\mathcal{R}}>\frac{\mathcal{R}}{B_{13}} .$$

Furthermore, because

$$\left|\frac{W_{21}-W_{32}}{W_{31}+W_{21}}\right|<1 ,$$

a necessary (but not sufficient) condition for the simultaneous inversion of levels (3,2) and (3,1) is the validity of the following inequality between the stimulated coefficients and the Raman rate

$$B_{13}>\mathcal{R}>B_{23} . \quad (5.7)$$

We note also that, in the large driving fields condition, we have

$$\frac{B_{23}}{\mathcal{R}}\approx\frac{\mathcal{R}}{B_{13}}\approx\frac{g_2^2}{g_1^2} , \quad (5.8)$$

so that the simultaneous inversion requirement takes the form

$$\frac{W_{21}-W_{32}}{W_{31}+W_{21}}>\frac{g_2^2}{g_1^2} . \quad (5.9)$$

We shall obtain this result again in Sec. VI through the more elegant procedure of the dressed-state formalism.

In the case of the Ξ system [see Eqs. (A2) in the Appendix] the results analogous to Eqs. (5.5) are

$$D_{21}=\frac{1}{3}\frac{\mathcal{R}(W_{31}+W_{32})-B_{23}(W_{21}+W_{31})}{2\mathcal{R}\gamma_{13}} , \quad (5.10a)$$

$$D_{32}=\frac{1}{3}\frac{\mathcal{R}(W_{21}+W_{31})-B_{12}(W_{31}+W_{32})}{2\mathcal{R}\gamma_{13}} , \quad (5.10b)$$

where

$$B_{12}=\frac{\gamma_{13}}{\gamma_{12}\gamma_{23}D}2g_1^2\left[\gamma_{23}+\frac{g_1^2}{\gamma_{13}}\right] , \quad (5.11a)$$

$$B_{23}=\frac{\gamma_{13}}{\gamma_{12}\gamma_{23}D}2g_2^2\left[\gamma_{12}+\frac{g_2^2}{\gamma_{13}}\right] , \quad (5.11b)$$

$$\mathcal{R}=\frac{2g_1^2g_2^2}{\gamma_{12}\gamma_{23}D} , \quad (5.11c)$$

and

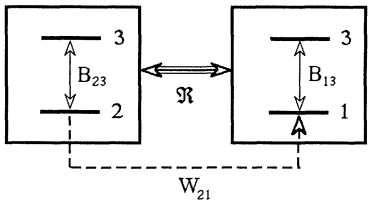

FIG. 8. Schematic representation of the interplay among the various transition rates in a Λ system.

$$D=\gamma_{13}+\frac{g_1^2}{\gamma_{23}}+\frac{g_2^2}{\gamma_{12}} . \quad (5.12)$$

In this case simultaneous inversion requires

$$\frac{W_{31}+W_{32}}{W_{21}+W_{31}}<\frac{\mathcal{R}}{B_{12}} \quad (D_{32}>0) \quad (5.13a)$$

and

$$\frac{W_{31}+W_{32}}{W_{21}+W_{31}}>\frac{B_{23}}{\mathcal{R}} \quad (D_{21}>0) \quad (5.13b)$$

or

$$\frac{\mathcal{R}}{B_{12}}>\frac{B_{23}}{\mathcal{R}} . \quad (5.13c)$$

The inequality (5.13c) is not satisfied, as we can easily verify from the definitions (5.11) of the stimulated and Raman rates. Thus, for the Ξ model either one or the other, but not both, of the allowed transitions can be simultaneously inverted.

It is possible to provide a simple interpretation of the

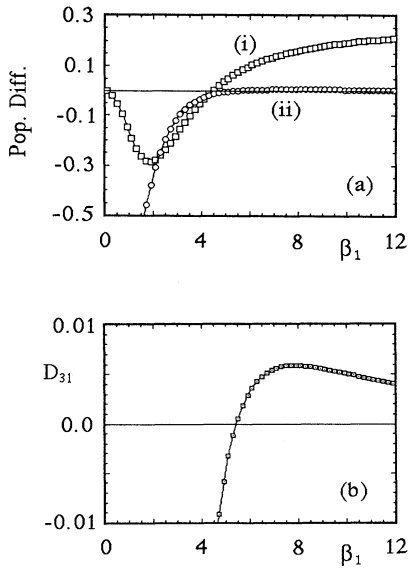

FIG. 9. The dependence of the population differences on the driving field β_1 in the Λ model. The scaled decay rates are $\tilde{W}_{21}=0.5$ and $\tilde{W}_{32}=0.2$. (a) shows the behavior of (i) D_{32} and (ii) D_{31}; (b) is an enlargement of (a) showing D_{31}.

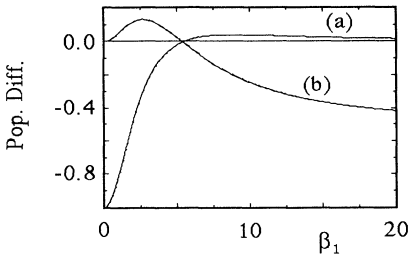

FIG. 10. The dependence of the population differences on the driving field β_1 in the Ξ model. The scaled transition rates are $\tilde{W}_{32}=0.5$ and $\tilde{W}_{31}=0.1$. Curve (a) shows the behavior of D_{21} and curve (b) shows D_{32}.

process described by Eqs. (5.3) with the help of Fig. 8. The two boxes illustrate the dynamics of two fictitious two-level systems driven by the respective fields at the rates B_{23} and B_{31}. If the boxes were isolated, no inversion would be possible. However, they are coupled to each other by the Raman process (connecting solid line) which represents losses for both levels 1 and 2 under conditions where both pairs of levels are inverted. Further coupling between the boxes is provided by the incoherent decay rates which cause population flow between them (thus, for example, W_{21} transfers atoms from the lower level of the left box to the lower level of the box on the right). Under appropriate conditions and because of the Raman coupling, it becomes possible for states of simultaneous inversion to be established.

Figures 9 and 10 summarize the situation graphically. In Fig. 9(a) we display the steady-state population differences D_{32} and D_{31} for the Λ model for fixed values of the spontaneous relaxation rates and the Rabi frequency β_2 as functions of the Rabi frequency β_1 [Fig. 9(b) shows an expanded view of D_{31} to show that it also becomes positive]. For the selected parameters there exists a threshold value of β_1 where both populations become inverted [around $\beta_1=5$ in Fig. 9(a)]. Figure 10 shows the corresponding situation for the Ξ model. Here we see that for any value of β_2 only one pair of levels can be inverted; when, for example D_{21} becomes positive, D_{32} becomes negative and vice versa, in line with the analytic results discussed in this section.

VI. DRESSED-STATE DESCRIPTION OF THE SPECTRA—THE HIGH-INTENSITY LIMIT

One of the most inconvenient features of the formulation discussed in Sec. III is its failure to provide analytical information about the physics of the problem. The spectral formulas are very convenient for numerical investigations, but they are of no use to assess qualitative trends and behaviors by inspection. The problem, as already discussed in Ref. 6, is that the atomic basis adopted for the representation of the density operator is not very convenient to describe the coherent coupling induced among the levels by the driving fields.

A much more powerful approach[13] is to expand the atomic operators in the basis of the eigenstates of the interaction Hamiltonian (dressed atomic states). In this way the equations for the coherent part of the dynamics becomes trivial, and one only needs to cope with the cumbersome irreversible decay terms. In the high-intensity limit, when the Rabi frequencies of the fields become much larger than the incoherent decay rates (a more precise characterization of this limit will be provided below), the damping part of the master equation can be handled by approximate techniques, and the problem becomes soluble in closed analytic form.

It is not our intention to duplicate the discussion of Ref. 6 because the treatment of the Λ and Ξ models using the dressed-state formalism runs along very similar lines. Here we emphasize only the most relevant facts under resonance conditions. The eigenstates of the interaction Hamiltonians (2.2a) and (2.2b) for the Λ and Ξ models, respectively, are sets of three linear combinations of the energy eigenstates $|i\rangle$ $(i=1,2,3)$, and they are given by the formulas

$$|r\rangle_\Lambda=-(\sin\theta)|1\rangle+(\cos\theta)|2\rangle\ , \tag{6.1a}$$

$$|s\rangle_\Lambda=\frac{1}{\sqrt{2}}[(\cos\theta)|1\rangle+(\sin\theta)|2\rangle+|3\rangle]\ , \tag{6.1b}$$

$$|t\rangle_\Lambda=\frac{1}{\sqrt{2}}[(\cos\theta)|1\rangle+(\sin\theta)|2\rangle-|3\rangle]\ , \tag{6.1c}$$

and

$$|r\rangle_\Xi=-(\sin\theta)|1\rangle+(\cos\theta)|3\rangle\ , \tag{6.2a}$$

$$|s\rangle_\Xi=\frac{1}{\sqrt{2}}[(\cos\theta)|1\rangle+|2\rangle+(\sin\theta)|3\rangle]\ , \tag{6.2b}$$

$$|t\rangle_\Xi=\frac{1}{\sqrt{2}}[(\cos\theta)|1\rangle-|2\rangle+(\sin\theta)|1\rangle]\ , \tag{6.2c}$$

where the angle θ is connected to the ratio of the two Rabi frequencies according to the equation

$$\tan\theta=\frac{g_2}{g_1}\ . \tag{6.3}$$

The eigenvalues of the interaction Hamiltonian in both cases are

$$|r\rangle\rightarrow 0,\quad |s\rangle\rightarrow\hbar G,\quad |t\rangle\rightarrow-\hbar G\ , \tag{6.4}$$

where

$$G=(g_1^2+g_2^2)^{1/2}\ . \tag{6.5}$$

We see that the two driving-field amplitudes affect the dynamics of the dressed states only through the combination (6.5); for obvious reasons, we call G the effective Rabi frequency of the problem. Thus, when we talk about the high-intensity limit, we refer to a situation where G is sufficiently large in comparison with the incoherent decay rates of the atom, regardless of the relative magnitudes of g_1 and g_2, and therefore of the values of the angle θ that appears in Eqs. (6.1) and (6.2).

Just as in the case of the V model, the master equation in the interaction picture for both Λ and Ξ models is

$$\frac{\partial\rho'}{\partial t}=-\frac{i}{\hbar}[H_1',\rho']+\Lambda\rho' \ , \tag{6.6}$$

when projected on the basis of the dressed states, it becomes the sum of a very simple reversible part (because H_1' is diagonal) and a very cumbersome irreversible contribution whose explicit expression is best obtained by symbolic logic techniques (see discussion in Sec. V of Ref. 6). In the limit in which G is much larger than the atomic damping rates, the eight linearly independent matrix elements of ρ' in the dressed-state representation obey the approximation equation

$$\frac{\partial\boldsymbol{\psi}}{\partial t}=L_0\boldsymbol{\psi}(t)+\mathbf{I}_\infty \ , \tag{6.7}$$

where L_0 is a block-diagonal matrix and $\mathbf{I}_\infty$ is a constant vector. The relation between the components of the vector $\boldsymbol{\psi}(t)$ and the matrix elements of ρ', and the explicit forms of L_0 and $\mathbf{I}_\infty$ are listed in the Appendix for completeness. Equation (6.7) is accurate up to terms of order $1/G$, and therefore it represents an asymptotic approximation of the exact equations of motion.

The emission and absorption spectra can be handled in exactly the same way as in Sec. V of Ref. 6 and reduced to simple analytic expressions because of the block-diagonal nature of the matrix L_0. The correlation functions in Laplace space are elementary rational functions from which the spectrum can be obtained according to the recipe

$$S(\omega)=\mathrm{Re}\hat{\Gamma}^{\,\mathrm{incoh}}(z)|_{z=i(\omega-\omega_0)} \ . \tag{6.8}$$

We consider first the Λ model. The emission spectrum of the $3\rightarrow1$ transition is assigned by the correlation function

$$\hat{\Gamma}_{\Lambda1}^{\mathrm{incoh}}(z)=\tfrac{1}{4}(\cos^2\theta)\psi_\infty\left[\frac{1}{z_1-\gamma_1+2iG}+\frac{1}{z_1-\gamma_1-2iG}+\frac{2}{z_1-\gamma_4+\gamma_5}\right]$$
$$+\tfrac{1}{2}(\sin^2\theta)\psi_\infty\left[\frac{z_1-\gamma_2+iG}{(z_1-\gamma_2+iG)^2-\gamma_3^2}+\frac{z_1-\gamma_2-iG}{(z_1-\gamma_2-iG)^2-\gamma_3^2}\right] , \tag{6.9a}$$

and the one for the $3\rightarrow2$ transition by

$$\hat{\Gamma}_{\Lambda2}^{\mathrm{incoh}}(z)=\tfrac{1}{4}(\sin^2\theta)\psi_\infty\left[\frac{1}{z_2-\gamma_1+2iG}+\frac{1}{z_2-\gamma_1-2iG}+\frac{2}{z_2-\gamma_4+\gamma_5}\right]$$
$$+\tfrac{1}{2}(\cos^2\theta)\psi_\infty\left[\frac{z_2-\gamma_2+iG}{(z_2-\gamma_2+iG)^2-\gamma_3^2}+\frac{z_2-\gamma_2-iG}{(z_2-\gamma_2-iG)^2-\gamma_3^2}\right] , \tag{6.9b}$$

where

$$\psi_\infty=\frac{W_{21}\cos^4\theta}{W_{21}(\sin^4\theta+2\cos^4\theta)+W_{32}\cos^2\theta+W_{31}\sin^2\theta} \ , \tag{6.10}$$

and

$$\gamma_1=-\tfrac{1}{4}[W_{21}\sin^2\theta(1+\sin^2\theta)+W_{32}(2+\sin^2\theta)+W_{31}(2+\cos^2\theta)] \ , \tag{6.11a}$$

$$\gamma_2=-\tfrac{1}{4}\{W_{21}[1+\cos^2\theta(1+2\sin^2\theta)]+W_{32}+W_{31}\} \ , \tag{6.11b}$$

$$\gamma_3=-\tfrac{1}{2}W_{21}\cos^2\theta\sin^2\theta \ , \tag{6.11c}$$

$$\gamma_4=-\tfrac{1}{4}\{W_{21}[\sin^2\theta(1+\sin^2\theta)+2\cos^4\theta]+W_{32}(1+\cos^2\theta)+W_{31}(1+\sin^2\theta)\} \ , \tag{6.11d}$$

$$\gamma_5=\tfrac{1}{4}[W_{21}(\cos^2\theta\sin^2\theta-2\cos^4\theta)+W_{32}\sin^2\theta+W_{31}\cos^2\theta] \ . \tag{6.11e}$$

The symbols z_1 and z_2 have the same meaning as in Sec. III, while ψ_∞ denotes the stationary matrix elements ρ_{ss}' and ρ_{tt}' which are equal in the high-field limit. We note that, when $W_{21}\rightarrow0$ (a situation that was well verified in the experiments of Ref. 12), the stationary atomic population is fully trapped in the r state ($\rho_{ss}'=\rho_{tt}'=0$) and, of course, the total fluorescence vanishes.

Both $3\rightarrow1$ and $3\rightarrow2$ emission spectra consist of five well-resolved components. The central peak and the $\pm2G$ sidebands have Lorentzian shapes, while the $\pm G$ sidebands have a slightly more complicated structure, as we can easily see from Eqs. (6.9a), (6.9b), and (6.8). The full widths at half maximum of the central peak and the sidebands of the $3\rightarrow1$ spectrum are identical to the corresponding widths of the $3\rightarrow2$ profiles and are given by

$$\Delta\omega(\text{central peak})=2|\gamma_5-\gamma_4|=W_{21}\sin^2\theta+W_{32}+W_{31} \ , \tag{6.12a}$$

$$\Delta\omega(\pm G)=2\{-2\gamma_3^2+[4\gamma_3^4+(\gamma_2^2-\gamma_3^2)^2]^{1/2}\}^{1/2} \ , \tag{6.12b}$$

$$\Delta\omega(\pm2G)=2|\gamma_1| \ . \tag{6.12c}$$

The peak heights of the $3\rightarrow1$ emission spectrum are given by

$$P_\Lambda(\text{central peak})=\tfrac{1}{4}\cos^2\theta\frac{2}{|\gamma_5-\gamma_4|}\psi_\infty \ , \tag{6.13a}$$

$$P_\Lambda(\pm G)=\tfrac{1}{2}\sin^2\theta\left|\frac{\gamma_2}{\gamma_2^2-\gamma_3^2}\right|\psi_\infty\ , \tag{6.13b}$$

$$P_\Lambda(\pm 2G)=\tfrac{1}{4}\cos^2\theta\frac{1}{|\gamma_1|}\psi_\infty\ . \tag{6.13c}$$

Those of the $3\rightarrow 2$ spectrum are identical except for the replacements of $\sin\theta$ with $\cos\theta$, and vice versa.

The absorption spectra in the high-field limit, just as those of the V model, are composed of only two peaks, centered at a distance of $\pm G$ from the atomic resonance, whose profile (and thus linewidth) is identical to that of the $\pm G$ sidebands of the fluorescence spectrum. The absorption spectrum can be negative (real absorption) or positive (gain) with a peak value given by

$$P_{\rm abs}(\pm G)=\tfrac{1}{2}\sin^2\theta(1-3\psi_\infty)\left|\frac{\gamma_2}{\gamma_2^2-\gamma_3^2}\right|\ , \tag{6.14}$$

whose sign is controlled by the quantity $(1-3\psi_\infty)$. It is easy to verify that

$$1-3\psi_\infty=\rho'_{rr}-\rho'_{ss}=\rho'_{rr}-\rho'_{tt}\ , \tag{6.15}$$

so that a growth of the weak probe requires inversion between the dressed states r and s (or t). Furthermore, with the help of Eq. (6.10), the gain condition $(1-3\psi_\infty)>0$ can also be cast into the form

$$\frac{g_2^2}{g_1^2}\le\frac{W_{21}-W_{32}}{W_{31}+W_{21}}\ , \tag{6.16}$$

which is identical to Eq. (5.9) obtained through an entirely different procedure.

The formulas for the Ξ model are quite similar to those of the Λ model, with enough differences, however, that it is necessary to summarize them separately. The emission spectrum of the $2\rightarrow 1$ transition is given by the correlation function

$$\hat{\Gamma}^{\rm incoh}_{\Xi 1}(z)=\tfrac{1}{4}\psi_\infty\cos^2\theta\left[\frac{1}{z_1-\gamma_1+2iG}+\frac{1}{z_1-\gamma_1-2iG}+\frac{2}{z_1-\gamma_4+\gamma_5}\right]$$
$$+\tfrac{1}{2}\psi_\infty\sin^2\theta\left[\frac{z_1-\gamma_2-iG}{(z_1-\gamma_2-iG)^2-\gamma_3^2}+\frac{z_1-\gamma_2+iG}{(z_1-\gamma_2+iG)^2-\gamma_3^2}\right]\ . \tag{6.17a}$$

For the $3\rightarrow 2$ decay we have instead

$$\hat{\Gamma}^{\rm incoh}_{\Xi 2}(z)=\tfrac{1}{4}\psi_\infty\sin^2\theta\left[\frac{1}{z_2-\gamma_1+2iG}+\frac{1}{z_2-\gamma_1-2iG}+\frac{2}{z_2-\gamma_4+\gamma_5}\right]$$
$$+\tfrac{1}{2}(1-2\psi_\infty)\cos^2\theta\left[\frac{z_2-\gamma_2+iG}{(z_2-\gamma_2+iG)^2-\gamma_3^2}+\frac{z_2-\gamma_2-iG}{(z_2-\gamma_2-iG)^2-\gamma_3^2}\right]\ , \tag{6.17b}$$

where

$$\psi_\infty=\frac{\tfrac{1}{2}(W_{31}\cos^4\theta+W_{32}\cos^2\theta)}{W_{31}(\tfrac{1}{2}\sin^4\theta+\cos^4\theta)+\tfrac{1}{2}W_{21}\sin^2\theta+W_{32}\cos^2\theta}\ , \tag{6.18}$$

and

$$\gamma_1=-\tfrac{1}{4}[W_{31}\sin^2\theta(1+\sin^2\theta)+3W_{32}\sin^2\theta$$
$$+W_{21}(2+\cos^2\theta)]\ , \tag{6.19a}$$

$$\gamma_2=-\tfrac{1}{4}\{W_{31}[1+\cos^2\theta(1+\sin^2\theta)]$$
$$+W_{32}(1+\cos^2\theta)+W_{21}\}\ , \tag{6.19b}$$

$$\gamma_3=-\tfrac{1}{2}W_{31}\cos^2\theta\sin^2\theta\ , \tag{6.19c}$$

$$\gamma_4=-\tfrac{1}{4}[W_{31}(\sin^2\theta+\sin^4\theta+2\cos^4\theta)$$
$$+W_{32}(1+\cos^2\theta)+W_{21}(1+\sin^2\theta)]\ , \tag{6.19d}$$

$$\gamma_5=\tfrac{1}{4}[W_{31}\cos^2\theta(\sin^2\theta-2\cos^2\theta)$$
$$+W_{32}(\sin^2\theta-2\cos^2\theta)+W_{21}\cos^2\theta]\ . \tag{6.19e}$$

As in the case of the Λ model, the symbol ψ_∞ denotes the stationary matrix elements ρ'_{ss} and ρ'_{tt} which are also equal to each other in the high-intensity limit. Contrary to the Λ model, however, ψ_∞ does not vanish if $W_{31}\rightarrow 0$ so that complete trapping is impossible in this case.

Both $2\rightarrow 1$ and $3\rightarrow 2$ emission spectra consist of five symmetric components. The central peak and the outer sidebands have a Lorentzian shape; the inner sidebands have a more complex structure. The full width at half maximum of these spectral components are the same for both the $2\rightarrow 1$ and $3\rightarrow 2$ fluorescence processes and they are given by

$$\Delta\omega(\text{central peak})=W_{31}\sin^2\theta+W_{32}\sin^2\theta+W_{21}\ , \tag{6.20a}$$

$$\Delta\omega(\pm G)=2\{-2\gamma_3^2+[4\gamma_3^4+(\gamma_3^2-\gamma_2^2)^2]^{1/2}\}^{1/2}\ , \tag{6.20b}$$

$$\Delta\omega(\pm 2G)=\tfrac{1}{2}[W_{31}\sin^2\theta(1+\sin^2\theta)+3W_{32}\sin^2\theta$$
$$+W_{21}(2+\cos^2\theta)]\ . \tag{6.20c}$$

Their peak heights are given by

$$P_{21}(\text{central peak})=\tfrac{1}{2}\cos^2\theta\frac{\psi_\infty}{|\gamma_5-\gamma_4|}\ , \tag{6.21a}$$

$$P_{21}(\pm G)=\tfrac{1}{2}\sin^2\theta\psi_\infty\left|\frac{\gamma_2}{\gamma_2^2-\gamma_3^2}\right|, \tag{6.21b}$$

$$P_{21}(\pm 2G)=\tfrac{1}{4}\cos^2\theta\frac{\psi_\infty}{|\gamma_1|}, \tag{6.21c}$$

$$P_{32}(\text{central peak})=\tfrac{1}{2}\sin^2\theta\frac{\psi_\infty}{|\gamma_5-\gamma_4|}, \tag{6.21d}$$

$$P_{32}(\pm G)=\tfrac{1}{2}\cos^2\theta(1-2\psi_\infty)\left|\frac{\gamma_2}{\gamma_2^2-\gamma_3^2}\right|, \tag{6.21e}$$

$$P_{32}(\pm 2G)=\tfrac{1}{4}\sin^2\theta\frac{\psi_\infty}{|\gamma_1|}. \tag{6.21f}$$

A measure of the accuracy of these formulas, when compared with the results of the exact calculations described in Sec. III, is offered by the solid lines in Figs. 11(a) and 11(b) which show the variation of linewidths and peak heights for the $3\rightarrow 2$ spectrum as one varies the size of the Rabi frequency β_2. The structure of these equations also shows that the Ξ model allows linewidth variations with the strengths of the driving fields, but the most promising configuration for this type of investigation still appears to be the V model. In fact, in this case, as it was for the Λ system, the full width of the central peak is determined in part by field-dependent contributions and in part by field-independent components ($W_{32}+W_{31}$ for the Λ model and W_{21} for the Ξ model).

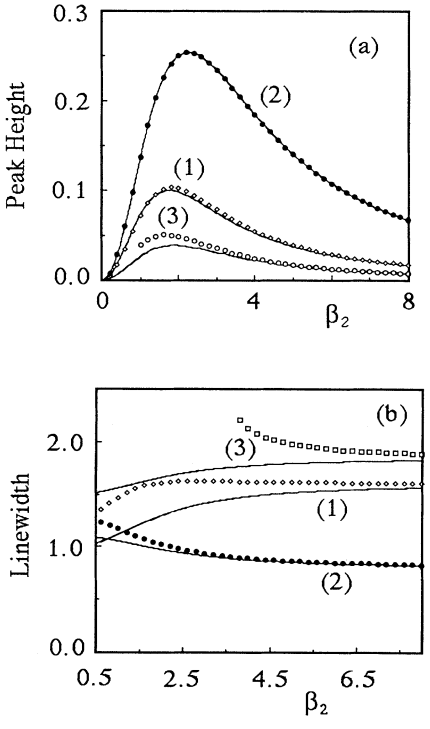

FIG. 11. Dependence of (a) the peak heights of the $3\rightarrow 2$ transition for the Ξ model and (b) the full width at half maximum on the driving field β_2. The scaled decay rates are $\tilde{W}_{31}=0.1$, $\tilde{W}_{32}=0.5$. The solid curves represent the results of the approximate analytic calculations, while the isolated points are derived from the theoretical formulas of Sec. III. The curves are labeled (1) for the central peak, (2) for the G peaks, and (3) for the $2G$ peaks.

The absorption spectra of the Ξ model in the high-intensity limit also reduces to two spectral components with a line shape which is the same as that of the $\pm G$ sidebands of the emission spectra, and the peak heights are given by

$$P_{21}(\pm G)=-\tfrac{1}{2}\sin^2\theta(1-3\psi_\infty)\left|\frac{\gamma_2}{\gamma_2^2-\gamma_3^2}\right|, \tag{6.22a}$$

$$P_{23}(\pm G)=\tfrac{1}{2}\cos^2\theta(1-3\psi_\infty)\left|\frac{\gamma_2}{\gamma_2^2-\gamma_3^2}\right|. \tag{6.22b}$$

Depending upon the sign of the quantity $(1-3\psi_\infty)$, one profile is positive while the other is negative. Thus, gain can be obtained in the vicinity of one transition frequency, but not both. The gain conditions for the two transitions are

$$\frac{W_{32}+W_{31}}{W_{31}+W_{21}}>\frac{g_2^2}{g_1^2} \quad \text{for the } 1\rightarrow 2 \text{ transition}, \tag{6.23a}$$

$$\frac{W_{32}+W_{31}}{W_{31}+W_{21}}<\frac{g_2^2}{g_1^2} \quad \text{for the } 2\rightarrow 3 \text{ transition}, \tag{6.23b}$$

in agreement with the results of Sec. V.

VII. CONCLUSIONS

In this paper we have completed a survey of the line shapes of the emission and absorption spectra produced by three-level atoms in which two pairs of dipole-allowed transitions are coupled by resonant or nearly resonant driving fields. This work began with a study of the V model, and is now completed with a detailed analysis of the Λ and Ξ configurations. The purpose of this conclusion section is to offer a comparison of our main results for each of the three models. Here we focus on three main issues: (i) population trapping, (ii) the emission spectra of spontaneous fluorescence, and (iii) the absorption spectra of a weak probe.

(i) Population trapping is a phenomenon that manifests itself with the appearance of reduced fluorescence from one of the excited states. This effect is especially obvious in the Λ system where, under ideal conditions (resonant interaction, homogeneous broadening, and $W_{21}\rightarrow 0$) the fluorescence intensity from the excited level 3 vanishes identically; in this case the atoms are distributed only in coherent superpositions of levels 1 and 2, while level 3 is empty. In the presence of leakage from level 2 ($W_{21}\neq 0$) the effect is reduced, and it can be eliminated altogether if W_{21} is sufficiently large (destruction of atomic coherence). Population trapping is also observable with V and Ξ systems, as shown in Figs. 3 and 4(a) of Ref. 6 for the V model, but not so clearly as with the Λ configuration.

(ii) The spontaneous distribution of the emitted fluorescence is very different from the expected results of the Wigner-Weisskopf theory, or even from the spectra that

emerge in the presence of a single driving field. In general, one can expect five spectral components, in resonance; they are distributed symmetrically around the atomic transition frequency, and are spaced from the center by approximately the effective Rabi frequency of the fields or twice this amount. There exist configurations in which the central peak and the $\pm 2G$ sidebands are the dominant features [see, for example, Fig. 2(a)], and conditions which favor the growth of the $\pm G$ peaks [see Fig. 2(c)].

The most interesting aspect of this phenomenon is the dependence of the full width at half maximum of the spectral components upon the relative strengths of the driving fields. With appropriate choices of the parameters this dependence can result in a strong linewidth reduction or broadening, relative to the Wigner-Weisskopf value. The best system for a demonstration of this effect appears to be the V model. The central peak of the $3 \rightarrow 1$ decay is governed by the approximate linewidth formula

$$\Delta\omega(\text{central peak}) = W_{31}\cos^2\theta + W_{21}\sin^2\theta \ , \tag{7.1}$$

where θ is defined as in Eq. (6.3). If $W_{21} \ll W_{31}$ and $g_2 \gg g_1$ the $3 \rightarrow 1$ linewidth is dominated by the rate W_{21}. Conversely, if one is monitoring the $2 \rightarrow 1$ decay with $g_1 \gg g_2$, the observed linewidth increases from W_{21} to nearly W_{31}.

Linewidth variations with the driving fields can be observed also with the other two models, but the expected changes are less easily observable. A particularly useful graphical demonstration of these behaviors are given by Figs. 8(b) of Ref. 6 (V model) and Fig. 11(b) of this paper (Ξ model).

(iii) The absorption spectra of a weak probe in the presence of the two driving fields reveal the presence of frequency ranges where the probe is attenuated and others where it is amplified. This is not very surprising because it had been predicted already and demonstrated experimentally with a driven two-level system. The main novelty exhibited by the three-level atoms is the appearance of a fully positive gain profile for the probe (see, for example, Fig. 4), and the simultaneous development of gain in the neighborhood of both allowed transitions for the V and Λ models. This phenomenon, which does not occur with the cascade configuration, develops in conjunction with the appearance of simultaneous stationary population inversion between both excited states and the lowest atomic level. The origin of the inversion can be traced to the interplay of ordinary stimulated emission, absorption, and spontaneous-decay processes with the Raman transitions, induced among the three atomic levels by the driving fields.

Apart from the intrinsic interest of the modified spontaneous-emission spectra of driven atoms, the presence of gain in three-level systems is perhaps the most promising feature for practical applications. It seems plausible, for example, that a cavity, with resonances at one of the peaks of the probe gain profile, should be able to support amplification. Perhaps, under special circumstances, this process may provide a useful mechanism for the enhancement of weak signals.

ACKNOWLEDGMENTS

We are grateful to Professor M. O. Scully for useful discussions and suggestions.

APPENDIX

We consider first the Λ model. The equations of motion of the density-matrix elements in the interaction picture follow from Eqs. (2.2a) and (2.3), in addition to the definitions (2.4) and (2.5). The explicit form of the population equations is

$$\dot{\rho}'_{11} = -ig_1(\rho'_{31}e^{-i\Delta_1 t} - \rho'_{13}e^{i\Delta_1 t}) + W_{21}\rho'_{22} + W_{31}\rho'_{33} - (W_{12} + W_{13})\rho'_{11} \ , \tag{A1a}$$

$$\dot{\rho}'_{22} = -ig_2(\rho'_{32}e^{-i\Delta_2 t} - \rho'_{23}e^{i\Delta_2 t}) + W_{12}\rho'_{11} + W_{32}\rho'_{33} - (W_{21} + W_{23})\rho'_{22} \ , \tag{A1b}$$

$$\dot{\rho}'_{33} = -i[g_1(\rho'_{13}e^{i\Delta_1 t} - \rho'_{31}e^{-i\Delta_1 t}) + g_2(\rho'_{23}e^{i\Delta_2 t} - \rho'_{32}e^{-i\Delta_2 t})] + W_{13}\rho'_{11} + W_{23}\rho'_{22} - (W_{31} + W_{32})\rho'_{33} \ . \tag{A1c}$$

For the polarization equations we have

$$\dot{\rho}'_{12} = -i(g_1\rho'_{32}e^{-i\Delta_1 t} - g_2\rho'_{13}e^{i\Delta_2 t}) - \gamma_{12}\rho'_{12} \ , \tag{A1d}$$

$$\dot{\rho}'_{13} = -i[g_1(\rho'_{33}e^{-i\Delta_1 t} - \rho'_{11}e^{-i\Delta_1 t}) - g_2\rho'_{12}e^{-i\Delta_2 t}] - \gamma_{13}\rho'_{13} \ , \tag{A1e}$$

$$\dot{\rho}'_{23} = -i[-g_1\rho'_{21}e^{-i\Delta_1 t} + g_2(\rho'_{33}e^{-i\Delta_2 t} - \rho'_{22}e^{-i\Delta_2 t})] \ , \tag{A1f}$$

in addition to the Hermitian symmetry $\rho'_{ij} = (\rho'_{ji})^*$, where the symbols

$$\Delta_1 = \omega_{31} - \omega_1, \quad \Delta_2 = \omega_{32} - \omega_2$$

denote the frequency detuning parameters. We implement the regression theorem by using a set of eight linearly independent variables $\psi_i(t)$, which are connected to the density-matrix elements ρ'_{ij} by the following relations:

$$\rho'_{11} = 1 - \psi_4 - \psi_8, \quad \rho'_{12} = \psi_1 e^{-i(\Delta_1 - \Delta_2)t}, \quad \rho'_{13} = \psi_2 e^{-i\Delta_1 t} ,$$
$$\rho'_{21} = \psi_3 e^{i(\Delta_1 - \Delta_2)t}, \quad \rho'_{22} = \psi_4, \quad \rho'_{23} = \psi_5 e^{-i\Delta_2 t} , \tag{A2}$$
$$\rho'_{31} = \psi_6 e^{i\Delta_1 t}, \quad \rho'_{32} = \psi_7 e^{i\Delta_2 t}, \quad \rho'_{33} = \psi_8 \ .$$

Equation (2.6) for the vector $\boldsymbol{\psi}$ follows at once by direct substitution of Eqs. (A2) into Eqs. (A1). The result provides the explicit expressions for the matrix L and the inhomogeneous vector $\mathbf{I}$.

For the Ξ model, with the help of Eqs. (2.2b) and (2.3), the population equations are

$$\dot{\rho}'_{11} = -ig_1(\rho'_{21}e^{-i\Delta_1 t} - \rho'_{12}e^{i\Delta_1 t}) - \rho'_{11}(W_{12} + W_{13}) + \rho'_{22}W_{21} + \rho'_{33}W_{31} \ , \tag{A3a}$$

$$\dot{\rho}'_{22}=-i[g_1(\rho'_{12}e^{i\Delta_1 t}-\rho'_{21}e^{-i\Delta_1 t}) +g_2(\rho'_{32}e^{-i\Delta_2 t}-\rho'_{23}e^{i\Delta_2 t})] +\rho'_{11}W_{12}-\rho'_{22}(W_{21}+W_{23})+\rho'_{33}W_{32}\ , \tag{A3b}$$

$$\dot{\rho}'_{33}=-ig_2(\rho'_{23}e^{i\Delta_2 t}-\rho'_{32}e^{-i\Delta_2 t})+\rho'_{11}W_{13}+\rho'_{22}W_{23} -\rho'_{33}(W_{31}+W_{32})\ , \tag{A3c}$$

and the polarization equations take the form

$$\dot{\rho}'_{12}-i[g_1(\rho'_{22}-\rho'_{11})e^{-i\Delta_1 t}-g_2\rho'_{13}e^{i\Delta_2 t}]-\rho'_{12}\gamma_{12}\ , \tag{A3d}$$

$$\dot{\rho}'_{13}=-i(g_1\rho'_{23}e^{-i\Delta_1 t}-g_2\rho'_{12}e^{-i\Delta_2 t})-\rho'_{13}\gamma_{13}\ , \tag{A3e}$$

$$\dot{\rho}'_{23}=-i[g_1\rho'_{13}e^{i\Delta_1 t}+g_2(\rho'_{33}-\rho'_{22})e^{-i\Delta_2 t}]-\rho'_{23}\gamma_{23}\ , \tag{A3f}$$

with $\rho'_{ij}=(\rho'_{ji})^*$ and

$$\Delta_1=\omega_{21}-\omega_1,\quad \Delta_2=\omega_{32}-\omega_2\ .$$

The components of the vector ψ are defined by the transformation equations

$$\rho'_{11}=1-\psi_4-\psi_8,\quad \rho'_{12}=\psi_1e^{-i\Delta_1 t},\quad \rho'_{13}=\psi_2e^{-i(\Delta_1+\Delta_2)t}\ ;$$
$$\rho'_{21}=\psi_3e^{i\Delta_1 t},\quad \rho'_{22}=\psi_4,\quad \rho'_{23}=\psi_5e^{-i\Delta_2 t}\ , \tag{A4}$$
$$\rho'_{31}=\psi_6e^{i(\Delta_1+\Delta_2)t},\quad \rho'_{32}=\psi_7e^{i\Delta_2 t},\quad \rho'_{33}=\psi_8\ .$$

Again, Eq. (2.6) for the vector ψ follows at once by direct substitution of Eqs. (A4) into Eqs. (A3). The result provides the explicit expressions for the matrix L and the inhomogeneous vector $\mathbf{I}$ for the Ξ model.

The dressed-state representation for both models is governed by the equation of motion for the transformed density-matrix elements (6.7). The connecting relations between the components of ψ and the matrix elements of ρ' are

$$\psi_1=\rho'_{st},\quad \psi_2=\rho'_{sr},\quad \psi_3=\rho'_{rt},\quad \psi_4=\rho'_{ss}\ ,$$
$$\psi_5=\rho'_{tt},\quad \psi_6=\rho'_{rs},\quad \psi_7=\rho'_{tr},\quad \psi_8=\rho'_{ts}\ . \tag{A5}$$

The approximate form of the L matrix in the high-intensity limit for both models has the block-diagonal form

$$L_0=\begin{bmatrix}
(\gamma_1-2iG) & 0 & 0 & 0 & 0 & 0 & 0 & 0\\
0 & (\gamma_2-iG) & \gamma_3 & 0 & 0 & 0 & 0 & 0\\
0 & \gamma_3 & (\gamma_2-iG) & 0 & 0 & 0 & 0 & 0\\
0 & 0 & 0 & \gamma_4 & \gamma_5 & 0 & 0 & 0\\
0 & 0 & 0 & \gamma_5 & \gamma_4 & 0 & 0 & 0\\
0 & 0 & 0 & 0 & 0 & (\gamma_2+iG) & \gamma_3 & 0\\
0 & 0 & 0 & 0 & 0 & \gamma_3 & (\gamma_2+iG) & 0\\
0 & 0 & 0 & 0 & 0 & 0 & 0 & (\gamma_1+2iG)
\end{bmatrix}, \tag{A6}$$

where the decay rates γ_i $(i=1,..,5)$ for the two models are defined by Eqs. (6.11) and (6.19), respectively. The inhomogenous vector $\mathbf{I}_\infty$ has the same form also for both the Λ and the Ξ models; this is given by

$$\mathbf{I}_\infty=\begin{bmatrix}
0\\0\\0\\-(\gamma_4+\gamma_5)\psi_4(\infty)\\-(\gamma_4+\gamma_5)\psi_5(\infty)\\0\\0\\0
\end{bmatrix}. \tag{A7}$$

*Also at: Center for Advanced Studies, University of New Mexico, Albuquerque, NM 87131.

†Permanent address: Department of Mathematics, University of Arizona, Tucson, AZ 85721.

[1]C. R. Stroud, Jr., Phys. Rev. A **3**, 1044 (1971); F. Shuda, C. R. Stroud, Jr., and M. Hercher, J. Phys. B **7**, L198 (1974).

[2]W. Hartig and H. Walther, Appl. Phys. **1**, 171 (1973).

[3]F. Y. Wu, R. E. Grove, and S. Ezekiel, Phys. Rev. Lett. **35**, 1426 (1975); R. E. Grove, F. Y. Wu, and S. Ezekiel, Phys. Rev. A **15**, 227 (1975).

[4]See, for example, D. J. Wineland and W. M. Itano, Phys. Lett. **82A**, 75 (1981).

[5]See, for example, J. C. Bergquist, R. G. Hulet, W. M. Itano, and D. J. Wineland, Phys. Rev. Lett. **14**, 1699 (1986), and references therein.

[6]L. M. Narducci, M. O. Scully, G.-L. Oppo. P. Ru, and J. R. Tredicce, Phys. Rev. A **42**, 1630 (1990).

[7]V. Weisskopf and E. Wigner, Z. Phys. **63**, 54 (1930); **65**, 18 (1931).

[8]Y. Zhu, D. J. Gauthier, and T. W. Mossberg (private communication).

[9]B. R. Mollow, Phys. Rev. A **5**, 2217 (1972); S. Haroche and F. Hartmann, *ibid.* **6**, 1280 (1972); F. Y. Wu, S. Ezekiel, M. Ducloy, and B. R. Mollow, Phys. Rev. Lett. **38**, 1077 (1977); M. T. Gruneisen, K. R. MacDonald, and R. W. Boyd, J. Opt. Soc. Am. B **5**, 123 (1988).

[10]H. Haken, *Laser Theory,* in Handbuch der Physik Vol XXV/2c (Springer-Verlag, Berlin, 1970), p. 57.

[11]M. Lax, in *Statistical Physics, Phase Transitions, and Superfluidity,* edited by M. Chretien, E. P. Gross, and S. Deser (Gordon and Breach, New York, 1968), Vol. 2, p. 269.

[12]H. R. Gray, R. M. Whitley, and C. R. Stroud, Jr., Opt. Lett. **3**, 218 (1978).

[13]C. Cohen-Tannoudji and S. Reynaud, J. Phys. B **10**, 345 (1977); **10**, 365 (1977); **10**, 2311 (1977).